RESEARCH PAPER

Effect of adding Nanoclay (Cloisite-30B) on the Proton Conductivity of Sulfonated Polybenzimidazole

***Hashem Ahmadizadegan** **

Department of Chemistry, Isfahan University of Technology, Isfahan, Iran

ARTICLE INFO

Article History:
Received 21 March 2017
Accepted 8 May 2017
Published 10 June 2017

Keywords:
Ion Exchange
Nanocomposite
Organoclay
Sulfonated Polybenzimidazole

ABSTRACT

A novel sulfonated polybenzimidazole/organoclay (Cloisite-30B) (SPBI/clay) nanocomposite membranes was successfully synthesized based on aromatic diacide (1) and diaminobenzidine. Nanocomposite membranes were fabricated using 1, 4-bis (hydroxymethyl) benzene (BHMB) as cross-linker, and Cloisite-30B organoclay as the pseudo cross-linker. The cross-linked SPBI/clay nanocomposite membranes were prepared via solution intercalation method. Participation of reactive organoclay in the cross-linking process was established from ion exchange capacity (IEC) measurements and FTIR studies. Wide angle X-ray diffraction (WAXD), field emission-scanning electron microscopy (FE-SEM), and transmission electron microscopy (TEM) techniques confirmed the presence of a combination of the intercalated and partially exfoliated clay platelets in the cross-linked SPBI/clay nanocomposite membrane. The cross-linked SPBI/clay nanocomposite membranes showed higher tensile strength, modulus and lower elongation at break compared to neat cross-linked SPBI. Water and methanol uptake studies revealed superior barrier properties of cross-linked SPBI/clay nanocomposite membranes compared to cross-linked SPBI. Furthermore, thermal stability, residual solvent in the membrane film, and structural ruination of membranes were analyzed by thermal gravimetric analysis (TGA). TGA data indicated an increase in thermal stability of the SPBI/clay nanocomposite membranes compared to the pure polymer. The oxidative stability of SPBI improved remarkably with cross-linking and subsequent clay addition. These improvements in the thermo-mechanical, barrier and oxidative stability of the membranes could be achieved without significantly affecting the protonic conductivity.

How to cite this article
Dehghankelishadi P, Dorkoosh FA. Pluronic based nano-delivery systems; Prospective warrior in war against cancer. Nanochem Res, 2017; 2(1):96-108. DOI: 10.22036/ncr.2017.01.009

INTRODUCTION

Polymer electrolyte membranes are currently under active development for electric vehicles, residential power sources, and portable devices. They have also attracted much attention due to their important applications in fuel cell systems. In the past few decades, various kinds of sulfonated aromatic polymers such as sulfonated poly (arylene ether)s like poly(ether ether ketone) PEEK and poly(sulfone), polybenzimidazole (PBI) and sulfonated polyimide (SPI) have been introduced for the development of high performing polymer electrolyte membranes as cheaper alternatives to the perfluorosulfonic acid (PFSA) membranes, Nafion, as the most common polymer for PEMFC application. Recent research has therefore focused on development of alternative membranes [1–4]. Fully aromatic polymers are currently being investigated due to their promising features, such as excellent thermal and mechanical stability, low cost and easy availability [5–7]. Furthermore, they

* Corresponding Author Emails: h.ahmadizadegan@ch.iut.ac.ir
h.ahmadizadegan.2005@gmail.com

can be easily functionalized for application as fuel cell membranes. Among aromatic polymers, hydrophobic poly (ether ether ketone) (PEEK) is the most studied case because of higher thermal and chemical stability, and also presenting an appreciable proton conductivity when sufficiently sulfonated [8–11]. Recently, a series of organic–inorganic composite membranes based on SPEEK have been reported [12]. The nanocomposite membranes of SPEEK with silicon oxide (SiO_2), titanium oxide (TiO_2), zirconium oxide (ZrO_2) and layered silicate materials [13–16] were reported to have reduced swelling without any appreciable reduction in conductivity. There are several factors that may contribute to the improvement of barrier properties and conductivity of the polymer electrolyte membrane (PEM), i.e., amount of filler loading, state of the dispersion of filler particles, length to width ratio of the filler particles and relative orientation of the filler particles [17]. Among the mentioned factors, the effect of filler loading has been identified as a crucial parameter that needs to be addressed as it affects the state of filler dispersion in polymer matrix, and it determines whether the composite formed is normal, intercalated or exfoliated composite. When an appropriate amount of filler is loaded, the aspect ratios of the inorganic fillers become significant to obtain membrane with high performance [18].

This study reports the influence of organoclay (Cloisite-30B) on the structural characteristics and the ion exchange capacity (IEC) measurements of conductive SPBI polymer membranes. Organoclay is used for enhancing strength and thermal resistance of membranes. It also exhibits a good affinity for some gas molecules and can be used as potential organoclay in nanocomposite proton conductivity membrane preparation. Reactive organoclay, Cloisite-30B, having surfactant containing hydroxyl groups can act as a pseudo cross-linker. Participation of organoclay in the cross-linking process was established from IEC measurements and FTIR spectroscopy. Nanocomposite membranes were fabricated by the solution casting method with different loadings of organoclay. Organoclay dispersion and morphology of the prepared nanocomposite were characterized using field emission-scanning electron microscopy (FE-SEM), and transmission electron microscopy (TEM) techniques. Characteristics of membranes such as thermal degradation and glass transition temperature (T_g) were evaluated by TGA and DSC. Furthermore, the variations of water and methanol uptake, protonic conductivity and oxidative stability of the nanocomposite membranes as a function of organoclay loading have also been studied.

EXPERIMENTAL

Equipments

Fourier-transform infrared (FT-IR) spectra were measured on a Nicolet Impact 410 FT-IR spectrometer. Proton nuclear magnetic resonance (^{1}H NMR) experiments were carried out on a Bruker 510 spectrometer using deuterated dimethyl sulfoxide as a solvent. Differential scanning calorimeter (DSC) measurements were performed on a Mettler Toledo DSC821e instrument at a heating rate of 20°C min^{-1} from 80°C to 300°C under nitrogen. Thermo gravimetric analysis (TGA) on a PerkinElmer Pyris-1 thermal analyzer system was employed to evaluate the thermal stability of the polymers. To remove water, the membranes were dried and kept in the TGA furnace at 150°C under a nitrogen atmosphere for 15min before testing. The samples were evaluated in the range of 100°C–800°C at a heating rate of 10°Cmin^{-1} under nitrogen atmosphere. Mechanical properties of the membranes were evaluated at room temperature on SHIMADZU AG-I 1KN at a strain rate of 2 mm min^{-1}, and a 500 N load cell was used. The samples were prepared by cutting the membranes in dumbbell shapes of 15 mm × 4 mm. At least three measurements for each membrane were taken and the average value calculated. The oxidative stability of the membranes was evaluated by immersing the samples in a Fenton's reagent (3% hydrogen peroxide (H_2O_2) containing 2 ppm ferrous sulfate ($FeSO_4$)) at 80°C. The stability was evaluated by recording the time when the membranes begin to break into pieces and start disappearing. The permeation cell was placed in a thermostatically controlled housing for maintaining isothermal measurement conditions. The reproducibility of the measurements was checked from three independent measurements using the same membrane, and it was better than ±5%.

Materials

4-fluorobenzonitrile, polyphosphoric acid (PPA), 4-(4-hydroxyphenoxy)phenol, N,N-dimethylacetamide (DMAc), sulfuric acid, ethanol, diaminobenzidine reagent, dimethyl sulfoxide (DMSO), and 1,4-bis (hydroxymethyl) benzene

(BHMB) were purchased from Aldrich (St. Louis, MO, USA) and used without any purification. Cloisite-30B used as organoclay in experiments was purchased from Southern Clay Products, Inc. The organic modifier (N-methyl tallow bishydroxyethyl quaternary ammonium) content in the organoclay was 0.9mequiv./g. A glass plate (20 cm × 28 cm) was used to prepare various polymer membranes.

Synthesis of monomer aromatic diacide (1)

As shown in Scheme 1, the monomer aromatic diacide (1) was synthesized using the following routine [19]. The yield was about 67% and the melting point was 286°C (DSC).

Synthesis of SPBI polymer [20]

2.57 g diaminobenzidine (12 mmol) and 5.31 g aromatic diacide (1) (12 mmol) were mixed with PPA (55 g) and placed in a round-bottom flask equipped with a reflux condenser with an inlet for nitrogen. The mixture was heated to 190 °C for 22 h. The polymerized PBI powder was collected and then dissolved in DMAc to prepare 10 wt% of the PBI solution. Incompletely dissolved PBI powder in DMAc was removed by a simple centrifugation step. To improve ion conductivity, the PBI film was treated with 98 wt% sulfuric acid at room temperature for three days (sulfonated-PBI, s-PBI membrane). This SPBI film was washed with ethanol and subsequently dried at 60 °C for 24 h (Scheme 1).

Synthesis of SPBI/Organoclay nanocomposite membrane

Cloisite-30B organoclay (1, 3 and 5weight% with respect to SPBI) was suspended in DMAc and vigorously stirred at 30 ◦C for 24 h. 10% SPBI by weight was dissolved in the same solution at 60 ◦C under stirring. The cross-linker, BHMB, was then added at a concentration of 1mol/mol repeat unit in the same solution and stirred till dissolution. The composite solution was then sonicated for 4 h and cast on a glass plate (Scheme 2). The film was then dried under ambient conditions for 2 days and then cured under vacuum at different temperatures. The sequence of heating was: 50 ◦C for 2 h, 100 °C for 2 h, 120 °C for 2 h and 135 °C for 24 h. [21]. To compare the properties of the cross-linked SPBI/clay nanocomposite membranes, pristine SPBI and neat 1MBHMB cross-linked membranes were prepared while adopting the same procedure. Cross-linked nanocomposite membranes with 1,

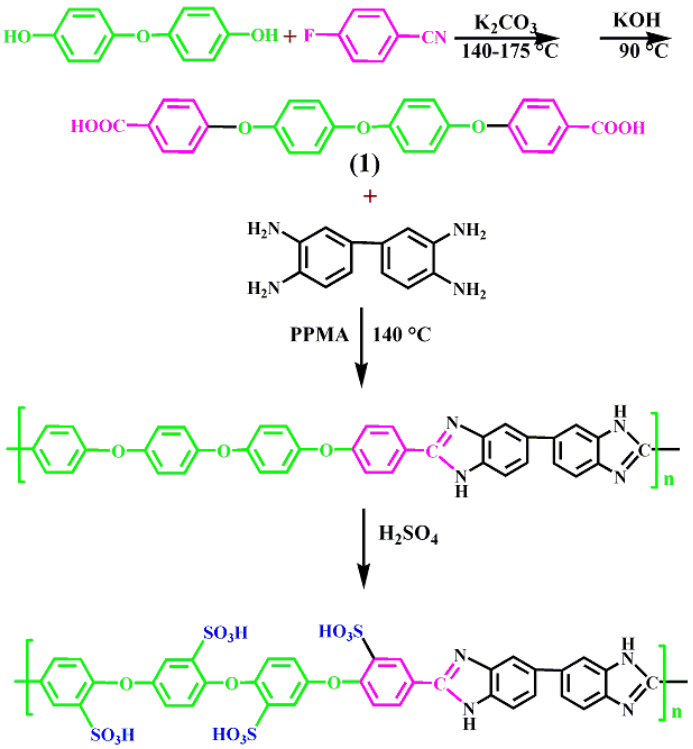

Scheme 1. Preparation of dibenzoic acid monomer and Synthesis of SPBI

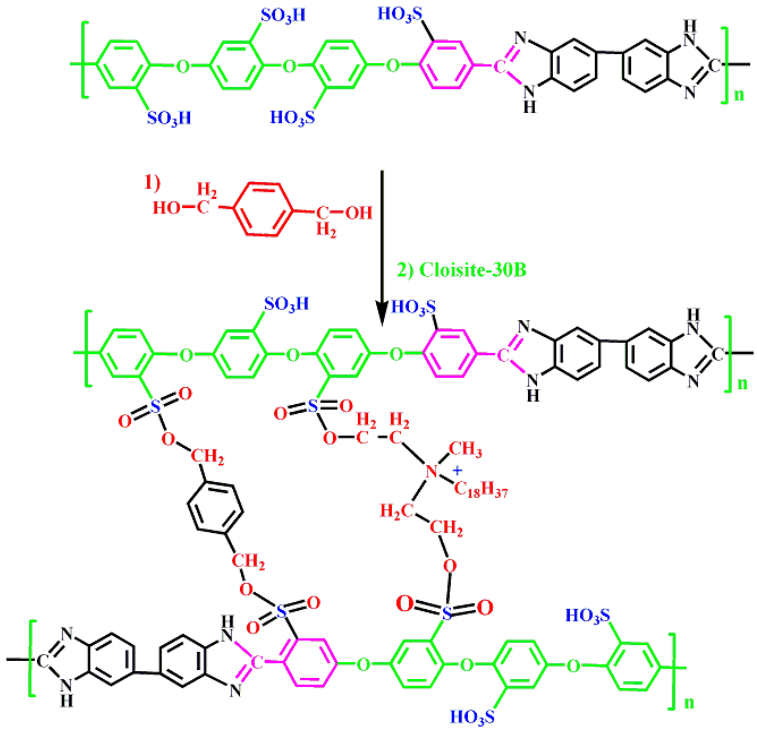

Scheme 2. Schematic of cross-linking of N-methyl tallow bis2-hydroxyethyl quaternary ammonium with BHMB cross-linked SPBI

3 and 5weight% of organoclay content have been nomenclatured as SPBI/clay 1%, SPBI/clay 3% and SPBI/clay 5%, respectively.

FT-IR data of pure SPBI (KBr, cm^{-1}): 3445 (s), 3435 (s), 3118 (w), 3065 (w), 1635 (s), 1525 (s) 1560 (m), 1556 (m), 1430 (w), 1055 (w), 850 (m), 645 (w).

FT-IR data of pure SPBI/organoclay (KBr, cm^{-1}): 3435 (s), 3356 (s), 3105 (w), 3012 (w), 1632 (s), 1550 (s) 15350 (m), 1526 (m), 1422 (w), 1052 (w), 752 (m), 635 (w).

RESULTS AND DISCUSSION

FT-IR of PBI and s-PBI Membranes

Fig. 1 shows the infrared (IR) spectra of PBI and

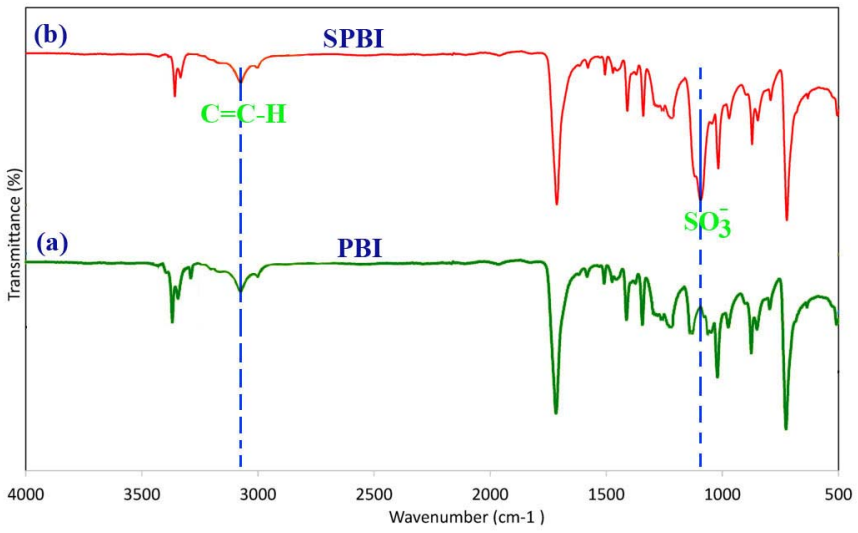

Fig. 1. Fourier transform infrared (FT-IR) spectra of polybenzimidazole (PBI) and sulfonated PBI (SPBI)

s-PBI with characteristic peaks at 3150–3500cm^{-1} for the N–H bond and at 1630 cm^{-1} for the C=N bond, respectively. The distinctive in-plane deformation peak of the imidazole ring was also observed at 1460 cm^{-1} [22]. Upon sulfonation, the s-PBI membrane clearly showed a new broad peak at 1053 cm^{-1}, corresponding to the symmetric stretch of the sulfonate group (SO_3^-).

^{1}H NMR spectrum of PBI

^{1}H NMR spectrum of PBI is shown in Fig. 2. All protons from 6.7 to 7.8 ppm with expected multiples and integrations are consistent with the proposed chemical structures of PBI. The signal of –NH in the imidazole ring was not obvious due to a strong proton exchange with the trace amount of water in the solvent. In addition, the chemical structure of PBI was also confirmed by its ^{1}H NMR spectrum (Fig. 2), which was consistent with the proposed chemical structures of PBI.

FT-IR spectroscopy of SPBI/Organoclay nanocomposite membrane

In this article, we used Cloisite-30B (clay modified with N-methyl tallow bishydroxyethyl quaternary ammonium) as an organoclay. Participation of hydroxyl groups of the organic modifier of the organoclay in the cross-linking process was evidenced by FT-IR spectroscopy and ion exchange capacity measurements. Fig. 3 shows the normalized FT-IR spectra of pure SPBI and cross-linked SPBI/organoclay nanocomposite membranes with varied organoclay content. In order to quantify the effect of reactive organocaly content on the hydroxyl peak intensity, the spectra were normalized w.r.t. The peak at 1220 cm^{-1} is corresponding to the –S=O stretching peak. A decrease in intensity of the free hydroxyl group band area of the pure SPBI was observed upon cross-linking with 1M BHMB, indicating that the cross-linker BHMB has consumed a fraction of SO_3H group during the cross-linking process. Furthermore, a monotonic decrease in the intensity of the free –OH group was observed with increasing clay loading. Fig. 3 compares the variation in the theoretical –OH group band intensity with organoclay loading (assuming only dilution effect) and the experimental findings of the variation in the –OH group spectral intensity. The decrease in the experimental intensity was found to be more than what would have occurred as a result of mere dilution effect of clay loading, implying that hydroxyl groups of the organoclay have participated in the cross-linking process.

Wide angle X-ray diffraction (WAXD), FE-SEM and TEM study of SPBI/Organoclay

Fig. 4 shows the WAXD plot of organoclay and cross-linked SPBI/Clay nanocomposite membranes. From the diffraction patterns, a diffraction maximum at 2θ value of 5.2◦, corresponding to a gallery spacing of 15.5 nm was observed for the organoclay. For the SPBI/Clay (1%) and SPBI/Clay (3%) nanocomposite membranes, no discernible diffraction peak corresponding to the $d_{(001)}$ basal spacing for the organoclay was observed, suggesting the possible exfoliation of clay platelets in the cross-linked SPBI

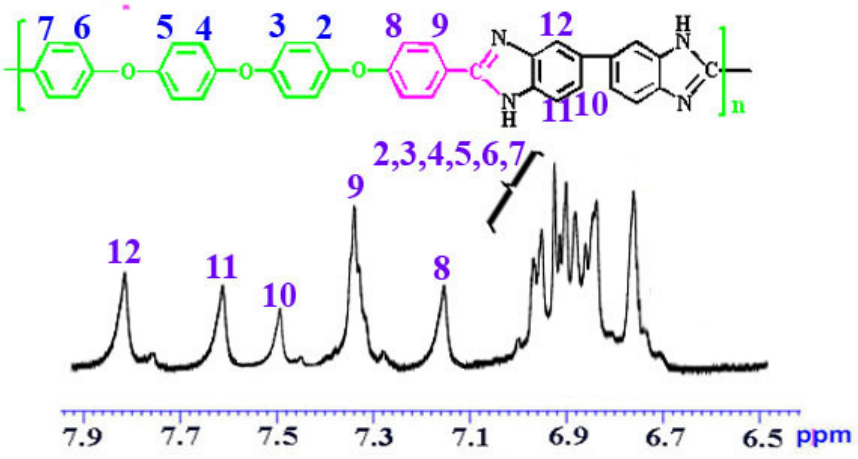

Fig. 2. ^{1}H-NMR (500 MHz) spectrum of PBI in DMSO-d6 at RT

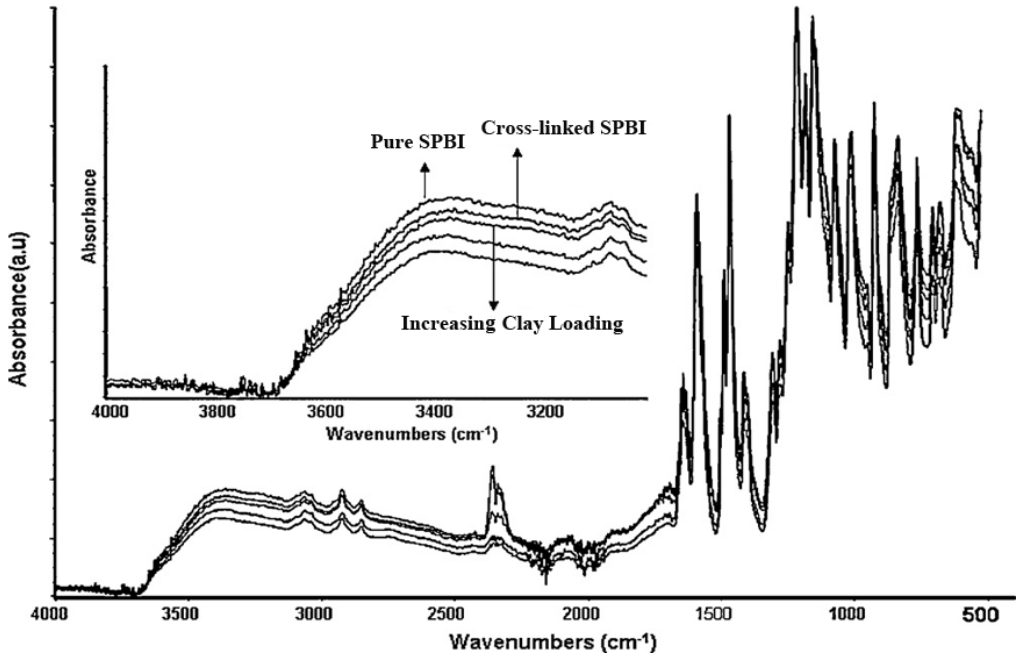

Fig. 3. Normalized FTIR spectra of pristine SPBI, neat cross-linked SPBI and cross-linked SPBI/clay nanocomposite membranes. The magnified OH stretching region is given in the inset

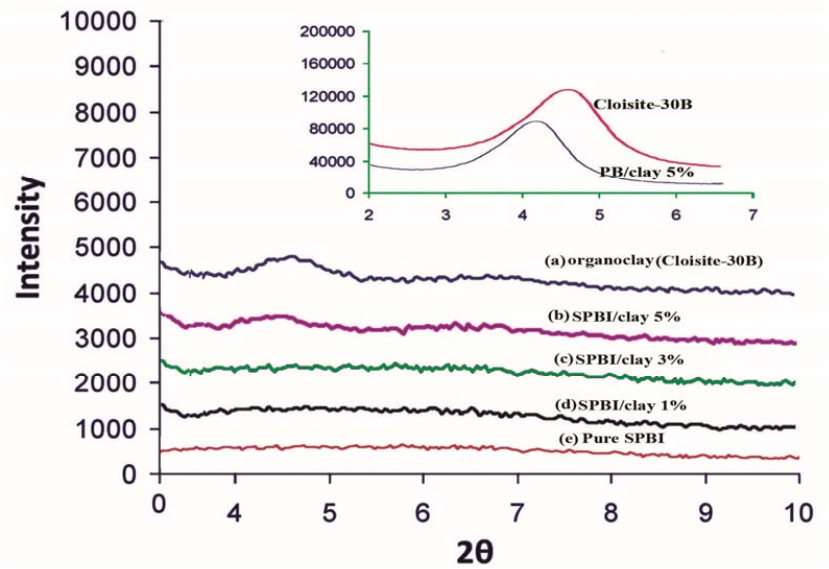

Fig. 4. WAXD plot of organoclay and cross-linked SPBI/clay nanocompositemem-branes

matrix. However, for SPBI/Clay (5%) a broad peak was noticed, with only a marginal shift towards lower 2θ value, indicative of possible intercalated clay dispersion morphology. A direct assessment of the clay dispersion morphology could be attained from TEM. Fig. 5a–c shows the TEM micrographs of the pure SPBI (a), SPBI/Clay (1%) (b) SPBI/Clay (3%) (c) and SPBI/Clay (5%) (d) nanocomposite membranes, respectively. In TEM micrographs, a mixture of intercalated and exfoliated morphologies was observed for SPBI/Clay (1%) (b). Predominantly intercalated clay dispersion morphology was observed in cases of SPBI/Clay (3%) (c) and SPBI/Clay (5%) (d). This indicated that the X-ray diffract gram did not represent the entire microstructure of the nanocomposite and

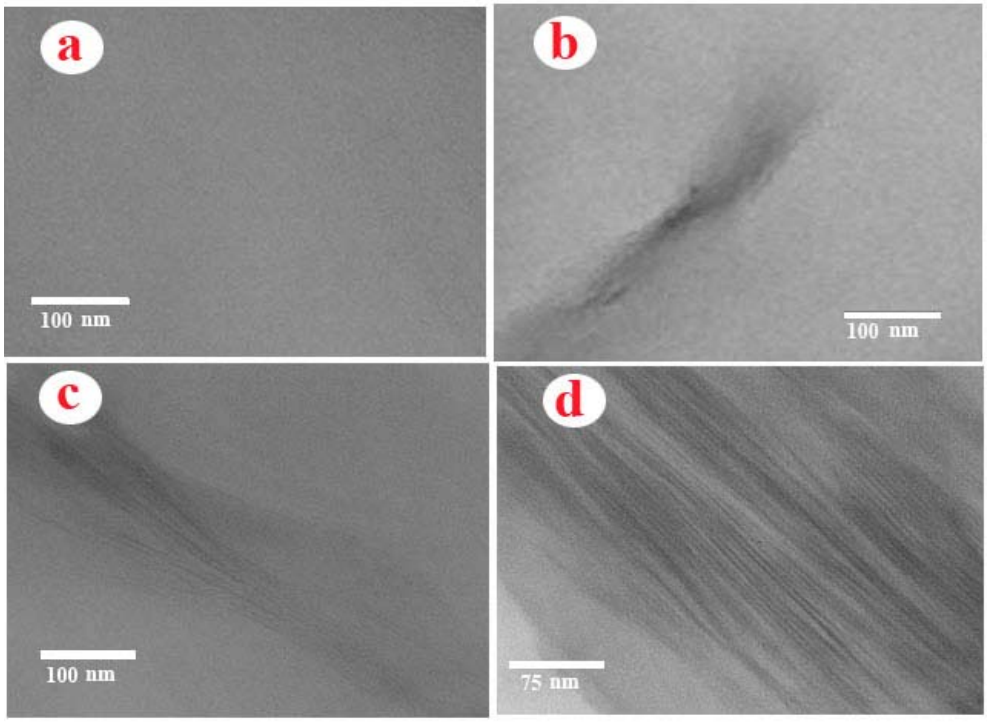

Fig. 5. TEM micrographs of (a) Pure SPBI, (b) SPBI/clay (1%)and (c) SPBI/clay (3%) and (d) SPBI/clay (5%) nanocomposite membranes at a magnification of 100 nm

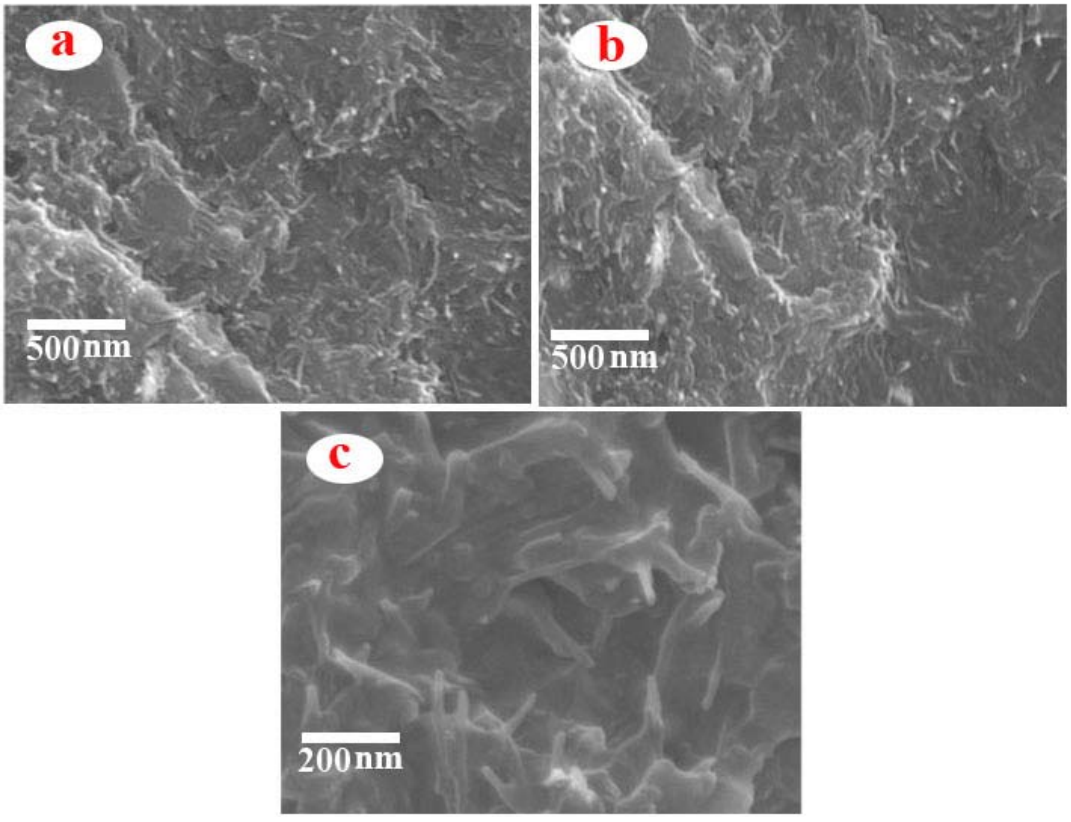

Fig. 6. FE-SEM (a-c) micrograph SPBI/clay (3%)

that a broad mixture of structures ranging from single layers to intercalated clay tactoids comprising different number of layers were present. Absence of peaks in the WAXD plot could be due to the random dispersion of the primary particles with different distances among clay and their heterogeneous microstructure. A direct assessment of the clay dispersion morphology could be obtained from transmission electron microscopy. Fig. 6a–c shows the FE-SEM micrographs of the SPBI/Clay (1%) (a) SPBI/Clay (3%) (b) and SPBI/Clay (5%) (c) nanocomposite membranes, respectively. These FE-SEM micrographs showed that the organoclay platelets have been uniformly distributed without agglomeration at low organoclay content SPBI/Clay (3%) Fig.6b. When the organoclay was increased to 3%, agglomeration of organoclay particles was observed as indicated in the FE-SEM micrograph. These results are also consistent to those obtained from the WARD and TEM measurements.

Thermal stability of SPBI/Organoclay

Thermal stability of the membranes in protonated form, consisting of pure SPBI and phosphoric acid doped blends (SPBI/Clay (1%), SPBI/Clay (3%) and SPBI/Clay (5%) were investigated by TGA in an argon atmosphere, at a scanning rate of 10 °C/min; the results are shown in Fig. 7. All of the samples showed a typical three-step degradation pattern. The first step of degradation in pure SPBI at about 115 °C is due to the loss of water molecules absorbed by the highly hygroscopic SO_3H groups. The second weight loss that started around 265 °C was assigned to the degradation of SO_3H groups. Finally the substantial weight loss at about 530 °C was attributed to the cleavage of the main polymer chain of SPBI/clay [23, 24]. The SPBI/clay nanocomposite membranes still had about 75 % weight remaining at 500 °C that shows the considerable thermal stability of the SPBI/clay nanocomposites. The TGA curve of pure SPBI also exhibited a three-step decomposition pattern. The first weight loss at about 110 °C is due to the loss of water absorbed from atmospheric humidity upon storing and preparing the SPBI sample for the TGA measurements, whereas the second one observed at about 255 °C, could be attributed to the degradation of imidazole rings, existing on the polymer chain. The third weight loss which began from about 410 °C corresponds to the cleavage of the SPBI backbone. As seen from the curves, all of the samples had a relatively high thermal stability.

As shown in Fig. 7, the initial decomposition temperatures of the pure SPBI and SPBI/clays are about 361°C. The char yield values of SPBI/clays have higher thermal stability than that of pure SPBI at 800 °C. Increasing the thermal stability in SPBI/clays is attributed to the high heat resistance exerted by the organoclay, because the organoclay has high thermal stability, so coupling of organoclay can improve the thermal stability of the SPBI/clays. This could be attributed to the intermolecular interactions between the functional groups of organoclay and SPBI. Table 1 shows the weight

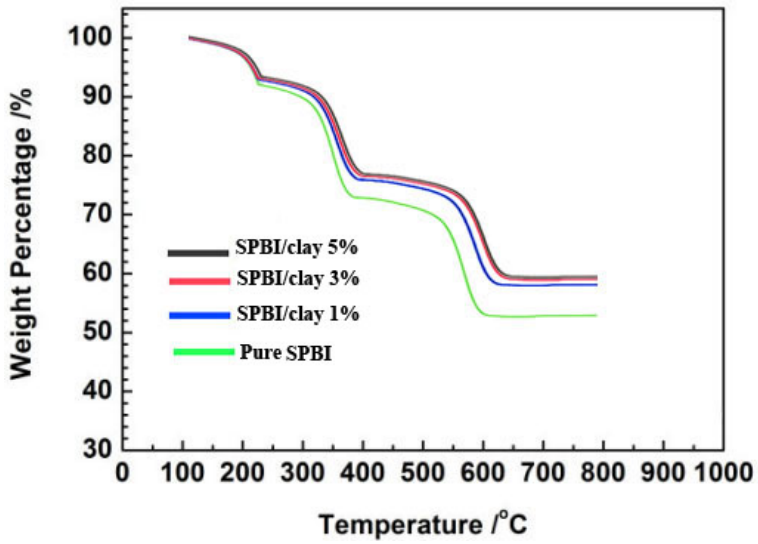

Fig. 7. TGA thermograms of Pure SPBI and SPBI/clays with different organoclay content

losses start up temperatures and also weight loss amounts of the samples at different temperatures.

Mechanical properties of SPBI/Organoclay

The mechanical stabilities of membranes (in acid form) were evaluated by means of tensile strength at ambient state; the resulting strain-stress curves are indicated in Fig. 8 and Table 2. All of the films were strong and flexible with a thickness of 45–55 micrometers. The films showed elongation at break of 7.33–11.31 %, illustrating that they have reasonably high values of mechanical properties. The average values and standard deviations of the neat SPBI and SPBI/clays tensile properties are summarized in Table 2. The tensile properties showed an increased modulus and strength of both SPBI/clays with 15 wt% organoclay compared to the pure SPBI. The effect of adding organoclay on SPBI matrix is related to the interactions of molecules in the nanohybrid films. Tensile properties of the hybrid films of SPBI/clays were studied by typical stress–strain curves. Specific values of the ultimate properties and the modulus of these samples are listed in Table2. In comparison, the pure SPBI with different amounts of organoclay has higher ultimate strength, higher initial Young's modulus, but lower ultimate elongation. The ultimate properties of the SPBI/clays are dependent on different parameters,

Table 1. Thermal characterizations of pure SPBI and SPBI/clay films

Polymer	T_5[a] (ºC)	T_{10}[a] (ºC)	Char yield (%)[b]	LOI[c]
Pure SPBI	255	301	51	37.93
SPBI/clay (1%)	256	310	58	40.71
SPBI/clay (3%)	257	312	59	41.12
SPBI/clay (5%)	258	315	60	41.52

[a]Temperature at which 5 and 10% weight loss were recorded by TGA at a heating rate of 10ºC/min in a nitrogen atmosphere.
[b] Percentage weight of material left undecomposed after TGA analysis at maximum temperature 800ºC in a nitrogen atmosphere.
[c] Limiting oxygen index (LOI) evaluating at char yield at 800ºC. LOI values were calculated based on Van Krevelen and Hoftyzer equation. LOI = 17.5 + 0.4 CR where CR = char yield.

Table 2. Mechanical properties for SPBI and SPBI/clay films

Material	Modulus[a](MPa)	Ultimate strength[b](MPa)	Ultimate elongation[c](%)
Pure SPBI	3565.11	225.65	11.31
SPBI/clay (1%)	3843.76	255.43	8.32
SPBI/clay (3%)	3976.85	265.88	7.85
SPBI/clay (5%)	4021.76	271.23	7.33

[a]Initial slope of the stress–strain curve. [b]Stress at break. [c]Elongation at break.

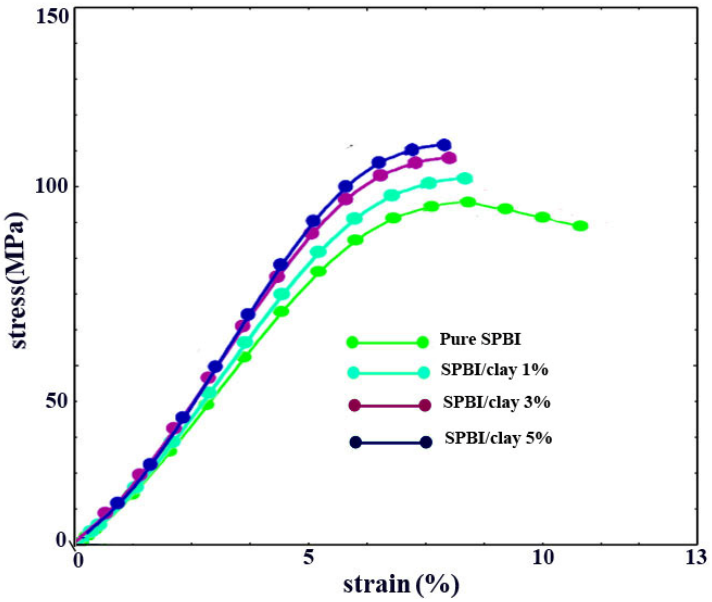

Fig. 8. Stress-strain curves of Pure SPBI and SPBI/clays with different organoclay content

such as the extent of bonding between the polymer matrix as continuous phase and organoclay as discontinuous phase, the surface area of the organoclay, and the arrangements between the SPBI/clays. The abovementioned results showed that the interactions between the SPBI matrix and organoclays are very important in the preparation of nanohybrid materials.

Water and Methanol uptake of SPBI/Organoclay

Water uptake plays an important role in proton exchange membranes because it is related to mechanical strength and proton conductivity [25]. The variation of water uptake of pure SPBI and cross-linked SPBI/clay nanocomposite membranes as a function of clay loading and temperature is shown in Table 3. The pristine SPBI showed water uptake of 50% at room temperature and dissolved at higher temperatures. At the same time, the neat cross-linked membrane showed a reduced water uptake at room temperature and only a moderate uptake of 30% at 80 °C. Due to the effect of organoclay loading, a significant decrease (12.1%) in the water uptake for SPBI/clay (1%) was observed compared to pure SPBI. With further increase in clay loading, even though the IEC value decreased and cross-link density increased, the water uptake increased significantly at higher temperatures. This could be attributed to the hydrophilicity of the Cloisite-30B organoclay, modified with hydroxyl functional group containing surfactant which can participate in strong hydrogen bonding with water [26].With increasing clay content in the cross-linked SPBI matrix, the residual reactive organoclay that does not participate in the cross-linking process increases due to the poor dispersibility of the clay platelets in the cross-linked SPBI matrix. Thus, the unreacted hydroxyl groups of the reactive organoclay renders the nanocomposite membranes more hydrophilic compared to the neat cross-linked SPBI membrane. Similar observations of higher water uptake for SPBI/Cloisite-15A clay nanocomposite membranes [27] and Krytox–Montmorillonite–Nafion® membranes [28] compared to parentmembranes have been reported. Furthermore, Pegoretti et al. [29] reported that among the various Cloisite clays, Cloisite-30B is the most hydrophilic based on vibration induced equilibrium contact angle measurements.

Methanol uptake in aqueous methanol solution was studied at 30 and 70 °C, respectively, and the results are presented in Table 3. The methanol uptake followed the same trend as water uptake. Cross-linking of the SPBI matrix drastically reduced the methanol uptake and among the nanocomposite membranes SPBI/clay (1%) showed the least methanol uptake as the case for water uptake.

Proton conductivity of SPBI/Organoclay

Having a proper proton conductivity is one of the most important features of a polymer electrolyte membrane. The proton conductivity measurements of the membranes in their acid form were evaluated by an electrochemical impedance spectroscopy technique, through the measurement of membrane resistance via an Auto lab impedance analyzer and a proton conductivity cell. Resistance and proton conductivity of the pure SPBI and SPBI/clay (1%) membranes were measured at ambient humidity (about 40 % RH) and a range of temperatures. The membrane resistance was obtained from Nyquist diagrams and their corresponding proton conductivities achieved from Eq. (1) are given in Table 4.

Table 3. Water and methanol uptake of crosslinked SPBI and cross-linked SPBI/clay nanocomposite membranes as a function of temperature.

Membrane	Water uptake (weight %)						Methanoluptake(weight%)	
	30	40	50	60	70	80	30	70
Pure SPBI	22	25	28	33	35	43	25	32
SPBI/clay (1%)	18	23	25	28	28	35	22	25
SPBI/clay (3%)	23	26	28	29	32	38	23	38
SPBI/clay (5%)	25	29	32	35	34	40	28	52

Table 4. Proton conductivity and weight loss (weight%) in Fenton's test of the membranes with clay content

Membranes	20 °C	40 °C	60 °C	80 °C	100 °C	120 °C	140 °C	Weight loss in Fenton's test (weight%)
Pure SPBI	8.01	8.25	10.75	16.22	25.87	35.77	39.98	2.25
SPBI/clay (1%)	7.93	8.05	9.04	15.32	23.04	34.95	35.97	1.55
SPBI/clay (3%)	9.25	9.21	12.55	18.85	27.33	38.78	42.35	1.23
SPBI/clay (5%)	10.22	10.54	18.27	22.37	30.78	45.37	48.88	0.88

Table 5. N_2 adsorption/desorption measurement results of pure SPBI, mesoporous organoclay and SPBI-Organoclay (3%)

Materials	S_{BET} (m^2/g)	D (nm)	V_t (cm^3/g)
Organoclay	225.43	3.45	0.38
SPBI-Organoclay (3%)	73.22	6.23	0.18
Pure SPBI	35.76	7.32	0.11

$$\sigma = \frac{l}{R \times A} \quad (1)$$

Where l is the distance (cm) between the Pt electrodes, which here is the same as the membrane thickness. R is the resistance value measured with Auto lab impedance analyzer, and A is the surface area (cm^2) required for a proton to penetrate into the membrane that is equal to the Pt platelets of the surface area. The impedance of each sample was measured three times to ensure good data reproducibility. Table 3 shows the conductivity of pure SPBI and cross-linked SPBI/clay nanocomposite membranes as a function of organoclay loading. Among the nanocomposite membranes, SPBI/clay (1%) showed lower conductivity compared to the pure SPBI, while SPBI/clay (5%) showed marginally higher conductivity. The higher conductivity of SPBI/clay (5%) membrane among nanocomposites could be caused by the conductivity of Cloisite-30B itself. It has been reported that the proton formed in the natural clay had a conductivity of 10^{-4} Scm^{-1} at room temperature [30].

Oxidative stability of SPBI/Organoclay

Ageing of membranes in fuel cell is a known phenomenon. The oxidative stability of membranes is used to determine the durability. In order to simulate the fuel cell environment, membranes were immersed in Fenton's reagent. Table 4 shows the weight loss of various types of membranes after exposure in Fenton's reagent for 1 h. Pure SPBI degraded and dissolved, whereas the nanocomposite membranes showed only 1.55% weight loss after 1 h of exposure. The weight loss of nanocomposite membranes decreased monotonically with clay loading, implying improved oxidative stability. Oxidative degradation is likely to occur at the carbon atom linking the ether bond of the SPBI matrix by attacking the hydroxyl radical due to high electron density at these positions [31, 32]. The higher oxidative stability of nanocomposite membranes could be attributed to the increase in degree of cross-linking induced by the reactive organoclay.

The N_2 adsorption/desorption isotherms and pore size distribution of mesoporous organoclay, SPBI-organoclay (3%) and Pure SPBI are listed in Table 5. These results prove that the organoclay and SPBI-organoclay are all mesoporous. However, compared with the mesoporous organoclay, the SPBI-organoclay has a small capillary condensation step, illustrating that the SPBI-organoclay may possess a hollow core or cavity caused by the packing of particles, and this result is also demonstrated by the two different pore size distribution peaks. As listed in Table 4, the mean pore diameter of SPBI-organoclay (3%) and mesoporous organoclay is 3.45 nm and 7.32 nm, respectively. The smaller mean pore diameter of SPBI-organoclay (3%) may be due to the existence of SPBI, which exists both in internal pores or channels and the surface of the organoclay. Although the pure SPBI has a similar isotherm with the SPBI-organoclay (3%), the specific surface area and mean pore diameter are all much smaller than that of the SPBI-organoclay (3%). According to the entire test results obtained, it is reasonable to presume that the SPBI has penetrated into the organoclay pores and channels; in other words, the SPBI-organoclay possesses a full interpenetrating structure.

CONCLUSIONS

A series of materials were synthesized in order to be used in the fabrication of proton exchange membranes. Nanocomposite membranes were fabricated using 1, 4-bis (hydroxymethyl) benzene (BHMB) as cross-linker and Cloisite-30B organoclay as the pseudo cross-linker. Incorporation of organoclay into cross-linked SPBI imparted additional degree of cross-linking to the membranes. Consequently, the cross-linked SPBI/clay nanocomposite membranes showed higher tensile strength, modulus and lower elongation at break compared to neat cross-linked SPBI. TGA studies revealed improved thermal stability of membranes with clay loading. Water and methanol uptake studies revealed superior barrier properties of cross-linked SPBI/clay nanocomposite membranes compared to cross-linked SPBI. Furthermore, the

oxidative stability of SPBI improved remarkably with cross-linking and subsequent clay addition. These improvements in the thermo-mechanical, barrier and oxidative stability of the membranes could be achieved without significantly affecting the protonic conductivity.

ACKNOWLEDGEMENTS

H. A. acknowledges financial support from Iran Nanotechnology Initiative Council (INIC).

CONFLICTS OF INTEREST

The author declares that he has no conflict of interest.

REFERENCES

1. Asensio JA, Sanchez EM, Gomez-Romero P. Proton-conducting membranes based on benzimidazole polymers for high-temperature PEM fuel cells. A chemical quest. Chemical Society Reviews. 2010;39(8):3210-39.
2. Tigelaar DM, Palker AE, He R, Scheiman DA, Petek T, Savinell R, et al. Synthesis and properties of sulfonated and unsulfonated poly(arylene ether triazine)s with pendant diphenylamine groups for fuel cell applications. Journal of Membrane Science. 2011;369(1–2):455-65.
3. Wang G, Xiao G, Yan D. Synthesis and properties of soluble sulfonated polybenzimidazoles derived from asymmetric dicarboxylic acid monomers with sulfonate group as proton exchange membrane. Journal of Membrane Science. 2011;369(1–2):388-96.
4. Liu B, Robertson GP, Kim D-S, Guiver MD, Hu W, Jiang Z. Aromatic Poly(ether ketone)s with Pendant Sulfonic Acid Phenyl Groups Prepared by a Mild Sulfonation Method for Proton Exchange Membranes. Macromolecules. 2007;40(6):1934-44.
5. Yang Y, Holdcroft S. Synthetic Strategies for Controlling the Morphology of Proton Conducting Polymer Membranes. Fuel Cells. 2005;5(2):171-86.
6. Hickner MA, Ghassemi H, Kim YS, Einsla BR, McGrath JE. Alternative Polymer Systems for Proton Exchange Membranes (PEMs). Chemical Reviews. 2004;104(10):4587-612.
7. Jung H-Y, Park J-K. Long-term performance of DMFC based on the blend membrane of sulfonated poly(ether ether ketone) and poly(vinylidene fluoride). International Journal of Hydrogen Energy. 2009;34(9):3915-21.
8. Zhao C, Wang Z, Bi D, Lin H, Shao K, Fu T, et al. Blend membranes based on disulfonated poly(aryl ether ether ketone)s (SPEEK) and poly(amide imide) (PAI) for direct methanol fuel cell usages. Polymer. 2007;48(11):3090-7.
9. Di Vona ML, Marani D, D'Ottavi C, Trombetta M, Traversa E, Beurroies I, et al. A Simple New Route to Covalent Organic/Inorganic Hybrid Proton Exchange Polymeric Membranes. Chemistry of Materials. 2006;18(1):69-75.
10. Marani D, Di Vona ML, Traversa E, Licoccia S, Beurroies I, Llewellyn PL, et al. Thermal Stability and Thermodynamic Properties of Hybrid Proton-Conducting Polyaryl Etherketones. The Journal of Physical Chemistry B. 2006;110(32):15817-23.
11. Ghosh P, Pathak A, Goyat M, Halder S. Influence of nanoparticle weight fraction on morphology and thermal properties of epoxy/TiO2 nanocomposite. Journal of Reinforced Plastics and Composites. 2012;31(17):1180-8.
12. Jung DH, Cho SY, Peck DH, Shin DR, Kim JS. Preparation and performance of a Nafion®/montmorillonite nanocomposite membrane for direct methanol fuel cell. Journal of Power Sources. 2003;118(1–2):205-11.
13. Song M-K, Park S-B, Kim Y-T, Kim K-H, Min S-K, Rhee H-W. Characterization of polymer-layered silicate nanocomposite membranes for direct methanol fuel cells. Electrochimica Acta. 2004;50(2–3):639-43.
14. Gaowen Z, Zhentao Z. Organic/inorganic composite membranes for application in DMFC. Journal of Membrane Science. 2005;261(1–2):107-13.
15. Hasani-Sadrabadi MM, Emami SH, Ghaffarian R, Moaddel H. Nanocomposite Membranes Made from Sulfonated Poly(ether ether ketone) and Montmorillonite Clay for Fuel Cell Applications. Energy & Fuels. 2008;22(4):2539-42.
16. Kim TW, Sahimi M, Tsotsis TT. Preparation and Characterization of Hybrid Hydrotalcite-Sulfonated Polyetheretherketone (SPEEK) Cation-Exchange Membranes. Industrial & Engineering Chemistry Research. 2009;48(21):9504-13.
17. Chang J-H, Park JH, Park G-G, Kim C-S, Park OO. Proton-conducting composite membranes derived from sulfonated hydrocarbon and inorganic materials. Journal of Power Sources. 2003;124(1):18-25.
18. Velmurugan R, Mohan TP. Epoxy-Clay Nanocomposites and Hybrids: Synthesis and Characterization. Journal of Reinforced Plastics and Composites. 2008;28(1):17-37.
19. Liu Y, Shi Z, Xu H, Fang J, Ma X, Yin J. Preparation, Characterization, and Properties of Novel Polyhedral Oligomeric Silsesquioxane–Polybenzimidazole Nanocomposites by Friedel–Crafts Reaction. Macromolecules. 2010;43(16):6731-8.
20. Xu H, Chen K, Guo X, Fang J, Yin J. Synthesis of novel sulfonated polybenzimidazole and preparation of cross-linked membranes for fuel cell application. Polymer. 2007;48(19):5556-64.
21. Hande VR, Rao S, Rath SK, Thakur A, Patri M. Crosslinking of sulphonated poly (ether ether ketone) using aromatic bis(hydroxymethyl) compound. Journal of Membrane Science. 2008;322(1):67-73.
22. Deimede V, Voyiatzis GA, Kallitsis JK, Qingfeng L, Bjerrum NJ. Miscibility Behavior of Polybenzimidazole/Sulfonated Polysulfone Blends for Use in Fuel Cell Applications. Macromolecules. 2000;33(20):7609-17.
23. Jaafar J, Ismail AF, Mustafa A. Physicochemical study of poly(ether ether ketone) electrolyte membranes sulfonated with mixtures of fuming sulfuric acid and sulfuric acid for direct methanol fuel cell application. Materials Science and Engineering: A. 2007;460–461:475-84.
24. Jin J, Song M, Yao KJ. A MTDSC analysis of phase transition in polyurethane–organoclay nanocomposites. Thermochimica Acta. 2006;447(2):202-8.
25. Zawodzinski TA, Davey J, Valerio J, Gottesfeld S. The water content dependence of electro-osmotic drag in proton-conducting polymer electrolytes. Electrochimica Acta.

1995;40(3):297-302.

26. Gosalawit R, Chirachanchai S, Shishatskiy S, Nunes SP. Krytox–Montmorillonite–Nafion® nanocomposite membrane for effective methanol crossover reduction in DMFCs. Solid State Ionics. 2007;178(29–30):1627-35.
27. Pegoretti A, Dorigato A, Brugnara M, Penati A. Contact angle measurements as a tool to investigate the filler–matrix interactions in polyurethane–clay nanocomposites from blocked prepolymer. European Polymer Journal. 2008;44(6):1662-72.
28. Lin Y-F, Yen C-Y, Ma C-CM, Liao S-H, Hung C-H, Hsiao Y-H. Preparation and properties of high performance nanocomposite proton exchange membrane for fuel cell. Journal of Power Sources. 2007;165(2):692-700.
29. Jiang R, Kunz HR, Fenton JM. Investigation of membrane property and fuel cell behavior with sulfonated poly(ether ether ketone) electrolyte: Temperature and relative humidity effects. Journal of Power Sources. 2005;150:120-8.
30. T.A. Zawodzinski Jr. TES, J.Davey,R. Jestel,C. Lopaz, J.Valerio, S.Gottes-feld. A Comparative Study of Water Uptake By and Transport Through Ionomeric Fuel Cell Membranes. J Electrochem Soc. 1993;140(7):1981-5.
31. Hubner G, Roduner E. EPR investigation of HO/ radical initiated degradation reactions of sulfonated aromatics as model compounds for fuel cell proton conducting membranes. Journal of Materials Chemistry. 1999;9(2):409-18.
32. Wang C, Chen W, Chen Y, Zhao X, Li J, Ren Q. New fluorinated poly(ether sulfone imide)s with high thermal stability and low dielectric constant. Materials Chemistry and Physics. 2014;143(2):773-8.